Journal of Materials Chemistry C

ROYAL SOCIETY OF CHEMISTRY

PAPER

View Article Online
View Journal | View Issue

Cite this: J. Mater. Chem. C, 2023, 11, 16390

Metal halides $RbCdCl_3:Sb^{3+}$ and $Rb_4CdCl_6:Sb^{3+}$ with yellow and cyan emissions obtained *via* a facile hydrothermal process

Dayu Huang,[ab] Pan Zheng,[ab] Ziyong Cheng,[ab] Qiuyun Ouyang,*[a] Hongzhou Lian*[ab] and Jun Lin*[ab]

Received 29th August 2023,
Accepted 10th November 2023

DOI: 10.1039/d3tc03098a

rsc.li/materials-c

It is of great interest to obtain multiple luminescent products from a single reaction, such as existing core–shell nanomaterials and heterojunction nanomaterials, all with the aim of enriching the photoelectric properties of the materials. Here, we report a hydrothermal approach for creating crystals of needle-shaped $RbCdCl_3:Sb^{3+}$ and bulk-shaped $Rb_4CdCl_6:Sb^{3+}$, two antimony doped-cadmium based metal halides. Two crystal materials with different shapes and phases can be synthesized simultaneously at the same stoichiometric ratio. $RbCdCl_3:Sb^{3+}$ is needle-shaped, whereas $Rb_4CdCl_6:Sb^{3+}$ is bulk-shaped. Under 320 nm excitation wavelength irradiation, blue emission (490 nm) of $Rb_4CdCl_6:Sb^{3+}$ and yellow emission (560 nm) of $RbCdCl_3:Sb^{3+}$ can be attained. Interestingly at low temperatures $RbCdCl_3:Sb^{3+}$ shows double peaked emissions (460 and 560 nm). This study investigates Sb^{3+}-doped $RbCdCl_3$ crystals that exhibit double luminescence as a result of intrinsic host self-trapped excitons and extrinsic dopant-induced self-trapped excitons (STEs), which are referred to as host STEs and Sb^{3+} dopant STEs, respectively. The construction of multicolor light-emitting devices is made possible by their color kinetics characteristics.

1. Introduction

With the gradual deepening of research based on metal halides and their applications, the requirements for the properties of metal halides will become more precise and demanding. Therefore, it can be expected that how to further develop the synthetic chemistry of metal halides will remain the core of their future research.[1–3] However, the synthetic chemistry of metal halides has already passed the early stage of exploration and has gradually formed a fixed synthesis mode and system. In order to break through the existing synthetic bottlenecks to achieve further development, it is necessary to systematically study the influence of various factors on the growth behaviour of metal halides during the synthesis process, so as to make relevant improvements. Phosphors with multiexcitonic emissions are necessary for building illumination devices like white light-emitting diodes (LEDs), as they improve their color rendering index performance.[4,5] Now, fluorescence/phosphorescence and exciton phase-space filling are the main methods used to produce multiexcitonic emissions in organic fluorophores and heterostructured semiconductor quantum dots. However, the main drawbacks of these types of multiexcitonic emissions are low controllability driven by the monodirectional intersystem crossover and low efficiency caused by quenching due to Auger recombination.[2,6] Because of their high tolerance for structural defects, which effectively prevents nonradiative energy losses, metal halides have recently demonstrated tremendous potential in lighting applications.[7] Given their great designability and tenability, metal halide variants with a vacancy-ordered structural arrangement have evolved in particular in recent years.[8] These so-called metal halides, such as Cs_2SnCl_6, Rb_4CdCl_6, and Cs_2ZrCl_6, have closely packed photogenerated charge carriers which foster charge recombination and light emission.[9–12] The addition of different dopant ions, which produce additional energy levels for sustaining excitons of adjustable energies in the host lattice, also makes it possible to easily adjust the emission lines of these crystals. For instance, Sb^{3+}-doped metal halides with coordination-dependent emission have been found to exhibit highly effective and low-toxic multicolor photoluminescence properties.[12–23] Although controlling the luminescence of metal halide crystals has been very effective, rational regulation of many excitonic emissions in a single reaction still has to be achieved. The dopant self-trapped

[a] Key Laboratory of In-Fiber Integrated Optics of Ministry of Education, College of Physics and Opotoelectronic Engineering, Harbin Engineering University, Harbin 150001, China. E-mail: qyouyang@hrbeu.edu.cn
[b] State Key Laboratory of Rare Earth Resource Utilization, Changchun Institute of Applied Chemistry, Chinese Academy of Sciences, Changchun 130022, P. R. China. E-mail: hzlian@ciac.ac.cn, jlin@ciac.ac.cn; Tel: +86-431-85698041

excitons (STEs) often predominate the emission spectra regardless of the excitation conditions, because of the strong interaction between the host and dopant STEs in a great deal of doped metal halide materials. In this study, two different types of metal halides ($RbCdCl_3$:Sb^{3+} and Rb_4CdCl_6:Sb^{3+}) are produced in a reactor under the same reaction conditions. $RbCdCl_3$:Sb^{3+} exhibits yellow emission (at about 560 nm) under 320 nm UV light irradiation, while Rb_4CdCl_6:Sb^{3+} exhibits cyanotic emission (at about 490 nm). $RbCdCl_3$:Sb^{3+} has another characteristic at a low temperature of −180 °C. A pure blue emission peak of the host appears, mixing with the yellow emission peak to form a single-phase white light emission. Therefore, the categorisation of multi-resonance emission in Sb^{3+} doped $RbCdCl_3$:Sb^{3+} and Rb_4CdCl_6:Sb^{3+} metal halides was investigated by spectroscopic measurements. We demonstrate that the different luminescence peaks of the $RbCdCl_3$:Sb^{3+} material resulting from host and dopant STEs are independent of each other. By precisely varying the temperature, dynamic color transmission can be achieved using multi-resonance emission.

2. Experimental

2.1 Chemicals

All chemical reagents were used without further purification: CdO (cadmium oxide, Aladdin), RbCl (rubidium chloride, Aladdin), HCl aqueous solution, $SbCl_3$ (antimony chloride, Aladdin). All reactions were performed under ambient conditions.

2.2 Synthesis of $RbCdCl_3$:Sb^{3+} and bulk-shaped Rb_4CdCl_6:Sb^{3+}

$RbCdCl_3$:Sb^{3+} and bulk-shaped Rb_4CdCl_6:Sb^{3+} were synthesized by using a hydrothermal method. RbCl (3 mmol), $SbCl_3$ (0.1–0.3 mmol) and CdO (1 mmol) were added into a 25 mL Teflon-lined autoclave. Then, 10 mL of HCl aqueous solution was added and heated at 150 °C for 2 h and then slowly cooled at 2 °C h^{-1} to room temperature. Finally, the obtained single crystal particles were washed two times with ethanol and dried at 80 °C for 1 h in a furnace. It is vital to note that only one reaction can produce two crystals.

2.3 Characterization

Phase identification was confirmed by X-ray diffraction using a D8 Focus diffractometer (Bruker) with Cu-Kα radiation (λ = 1.5405 Å). Analysis of the elements was performed using an energy-dispersive spectrometer equipped with a scanning electron microscope (S-4800; Hitachi, Japan). X-ray photoelectron spectroscopy (XPS) spectra were recorded employing a VG ESCALAB MK II electron spectrometer using the Mg Kα (1200 eV) line as an excitation source. Photoluminescence (PL) spectra and temperature-dependent (at −180 to 150 °C) PL spectra were recorded on a photoluminescence spectrophotometer with a 450 W xenon lamp as the excitation source equipped with a temperature controller (an Edinburgh Instrument FLS-920). Photoluminescence quantum yield (PLQY) values were collected on an absolute PL quantum yield measurement system (Hamamatsu Photonics K.K., C9920-02 Japan). The electroluminescence (EL) performance of the fabricated WLED devices was evaluated using a HAAS 2000 photoelectric measuring system (380–1100 nm, EVERFINE, China).

3. Results and discussion

Given their exceptional photoluminescence performance, metal halides are selected as host materials. To introduce dopant

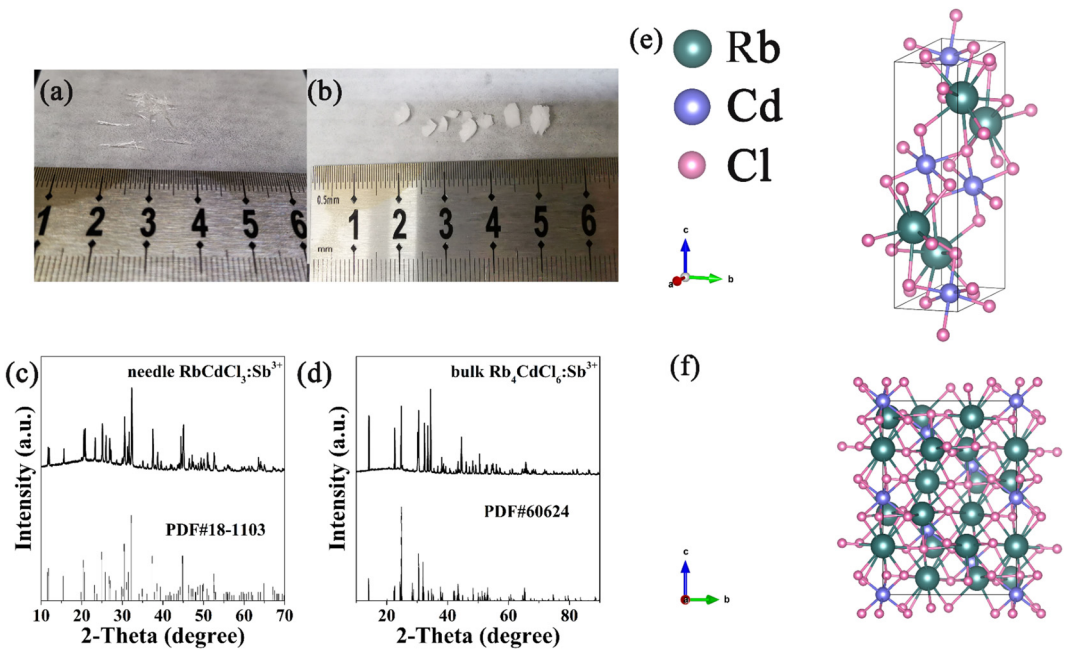

Fig. 1 (a) and (b) Photographs of needle-shaped $RbCdCl_3$:Sb^{3+} and bulk-shaped Rb_4CdCl_6:Sb^{3+}, respectively. (c) and (d) XRD patterns of $RbCdCl_3$:Sb^{3+} and Rb_4CdCl_6:Sb^{3+}, respectively. (e) and (f) Structural and compositional characterization of the $RbCdCl_3$:Sb^{3+} and Rb_4CdCl_6:Sb^{3+} crystals, respectively.

STEs by creating Sb^{3+}-based polyhedrons, the Sb^{3+} ion with an ns^2 electronic configuration was chosen. $SbCl_3$, CdO, RbCl, and HCl aqueous solutions were used as the starting materials in a co-precipitation process to create $RbCdCl_3$:Sb^{3+} and Rb_4CdCl_6:Sb^{3+} metal halides. The reaction process cools down very slowly. In the Experimental section, the synthesis process is described in extensive detail. After four days of controlled cooling, centimeter-sized crystals appeared. It is interesting to note that the synthetic crude product includes samples that resemble needle-shaped $RbCdCl_3$:Sb^{3+} and bulk-shaped Rb_4CdCl_6:Sb^{3+} (Fig. 1a). The needle-shaped $RbCdCl_3$:Sb^{3+} material has a length of approximately 1 cm. The bulk Rb_4CdCl_6:Sb^{3+} material's maximum width is roughly 0.5 cm. XRD was used to determine the material's phase (Fig. 1b and c). The needle-shaped $RbCdCl_3$:Sb^{3+} and bulk-shaped Rb_4CdCl_6:Sb^{3+} show distinct *Pnma* and $R\bar{3}c$ space groups (Fig. 1d and e). The structural

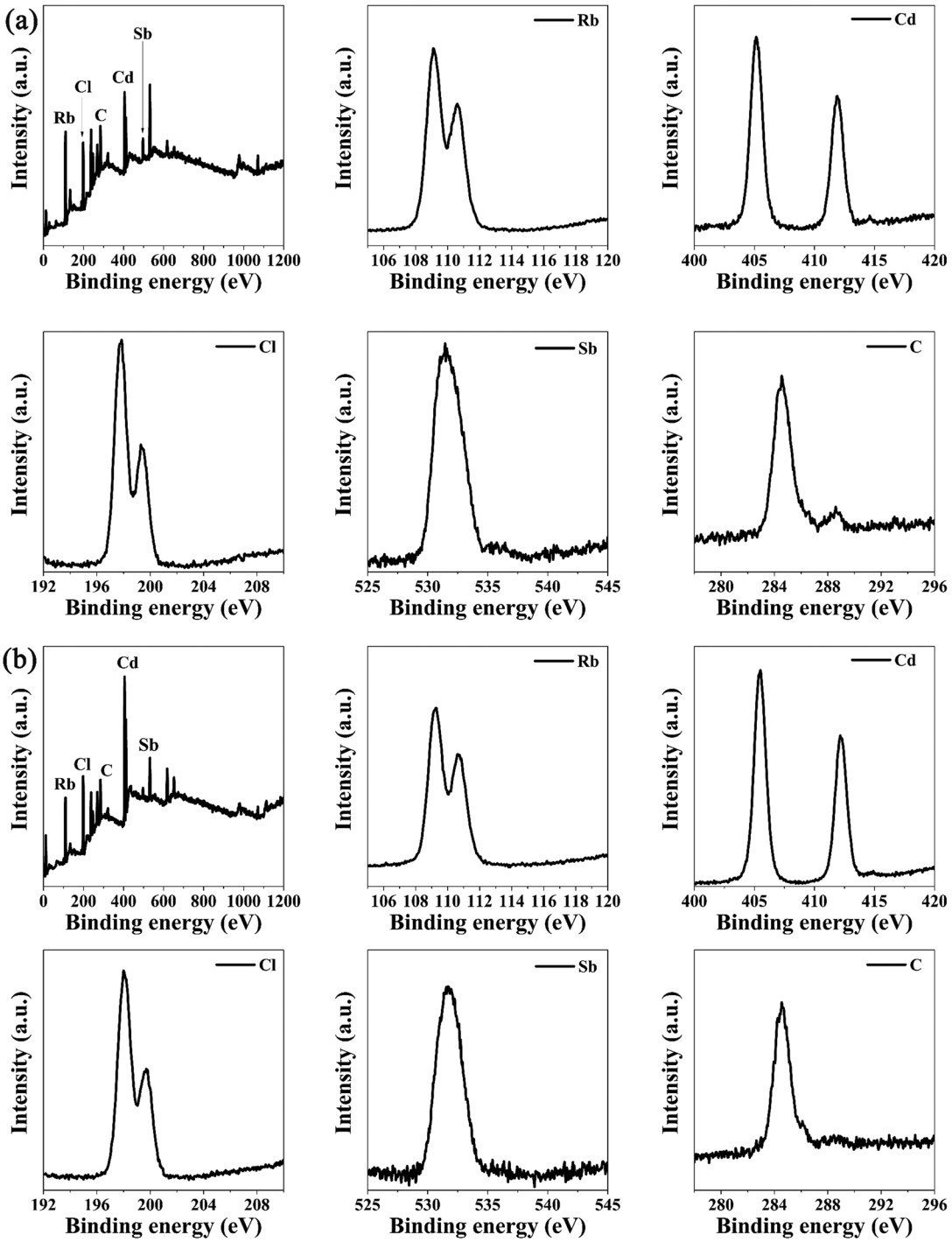

Fig. 2 (a) and (b) XPS spectra of the $RbCdCl_3$:Sb^{3+} and Rb_4CdCl_6:Sb^{3+} crystals, respectively.

components of $RbCdCl_3$ are depicted in Fig. 1d as $[CdCl_6]^{4-}$ and $[RbCl_9]^{8-}$ polyhedrons. It is known that Sb^{3+} ions preferentially occupy the 6-coordinated Cd^{2+} sites. The structural unit of Rb_4CdCl_6 is the polyhedron composed of $[CdCl_6]^{4-}$, $[RbCl_6]^{5-}$ and $[RbCl_8]^{7-}$ polyhedrons. With the development of a Cl vacancy ($[V_{Cl}]^{+}$) to maintain the charge balance, we determined that the Sb^{3+} dopant most likely existed as $[Sb_{Cd}]^{+}$.[9]

X-ray photoelectron spectroscopy (XPS), which verified the existence of Rb, Cd, Cl, and Sb elements in the $RbCdCl_3$:Sb^{3+} and Rb_4CdCl_6:Sb^{3+} crystals, also provided confirmation for the successful doping of Sb^{3+} ions (Fig. 2a and b). Fine peaks of Rb, Cd, Cl, and Sb are presented. The Rb $3d_{5/2}$ orbital binding energies of the two materials are between 108 and 112 eV. The binding energy of Cd $3d_{5/2}$ orbitals of both materials is located at 405 eV, and that of the other $3d_{3/2}$ orbitals is located at 412 eV. The binding energy of Cl $2p_{1/2}$ orbitals of the two materials is located at 200 eV, and that of the other $2p_{3/2}$ orbitals is located at 198 eV. The Sb $3d_{5/2}$ orbital binding energy of the two materials is located at 531 eV. Fig. 3a and b displays the SEM images of $RbCdCl_3$:Sb^{3+} and Rb_4CdCl_6:Sb^{3+}. $RbCdCl_3$:Sb^{3+} is primarily needle-like, with a minimum length of around 30 μm and a maximum length of about 1 cm. The elemental distribution obtained from SEM mapping images is displayed in order. Rb_4CdCl_6:Sb^{3+} has a significantly different shape. It appears as a bulk with a minimum width of more than 30 μm and a maximum width in centimeters, as in daylight photographs. The SEM mapping images of the Rb, Cd, Cl and Sb elements in Rb_4CdCl_6:Sb^{3+} are shown in Fig. 3, respectively.

The optical characteristics of the Sb^{3+}-doped $RbCdCl_3$:Sb^{3+} and Rb_4CdCl_6:Sb^{3+} crystals were then investigated. Photoluminescence excitation (PLE) demonstrated that Sb^{3+} doping adds extra excitation peaks in the 250–360 nm range to the sample (Fig. 4a and b). According to the results of the simulation, the large absorption peaks at 250–300 nm and 300–360 nm, respectively, were attributed to the $^1S_0$–$^1P_1$ and $^1S_0$–$^3P_1$ transitions of Sb^{3+} ions.[9] As a result, the Sb^{3+} dopant also increased the emission intensity of the $RbCdCl_3$ and Rb_4CdCl_6 host crystals. An optimal doping concentration of 20% was found by connecting the emission intensity and luminous quantum yield with the amount of Sb^{3+} present, at which point the greatest quantum yield of doping-induced emission was measured at 78%. Higher dopant concentrations may cause polyhedral cluster formation and a drop in the particle size and crystallinity, leading to a fall in emission intensity.

The photoluminescence (PL) spectra of the $RbCdCl_3$:Sb^{3+} and Rb_4CdCl_6:Sb^{3+} crystals were recorded in order to investigate the recombination processes in the Sb^{3+}-doped $RbCdCl_3$ and Rb_4CdCl_6 phosphors. The undoped Rb_4CdCl_6 phosphor had a weak emission peak centered at 490 nm under excitation at 297 nm, which was in line with a prior result.[11] $RbCdCl_3$ was much weaker and did not show the phenomenon of luminescence. Due to strong electron–phonon interactions in the metal halide materials with a soft lattice, the Rb_4CdCl_6 host STEs were thought to be responsible for the broad emission band with a significant Stokes shift of 193 nm. The $[CdCl_6]^{4-}$, $[RbCl_6]^{5-}$ and $[RbCl_8]^{7-}$ charge transition was attributed to the solitary peak at 490 nm in the emission spectra. Numerous instances of this charge transition were also seen in metal halides. In addition to the host excitation band at 290 nm, a novel excitation band centered at 320 nm was found for the $RbCdCl_3$:Sb^{3+} and Rb_4CdCl_6:Sb^{3+} crystals. The direct excitation of Sb^{3+} ions through the $^1S_0 \rightarrow {}^1P_1$ transition, which was also frequently observed in Sb^{3+}-doped metal halides such $RbCdCl_3$:Sb^{3+} and Rb_4CdCl_6:Sb^{3+}, was assigned to the

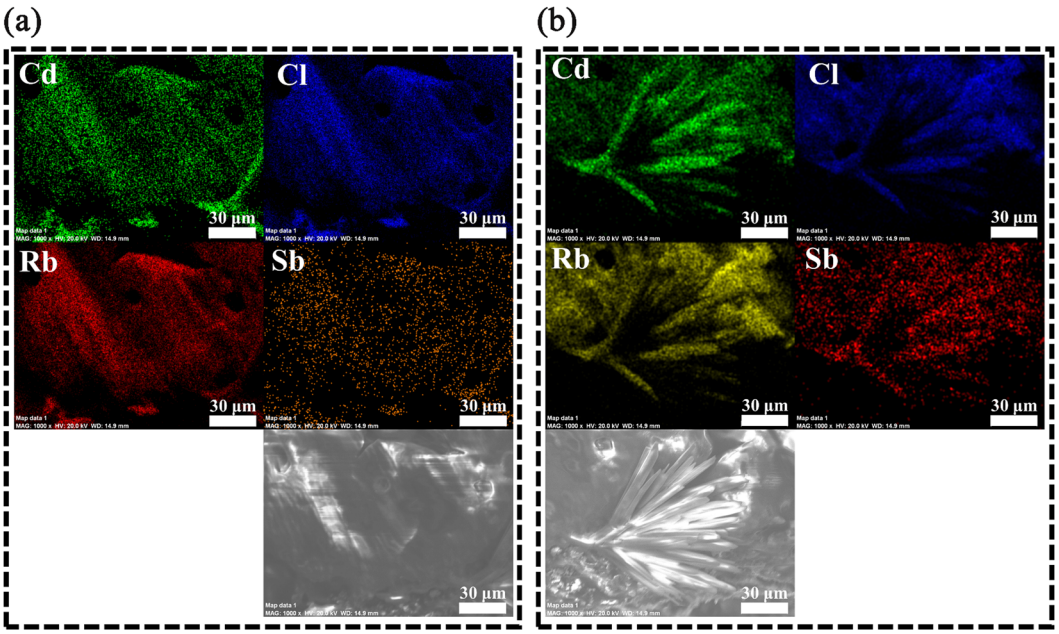

Fig. 3 (a) and (b) SEM images and elemental mapping of Rb_4CdCl_6:Sb^{3+} and $RbCdCl_3$:Sb^{3+} showing the uniform distribution of Cd, Cl, Rb and Sb elements.

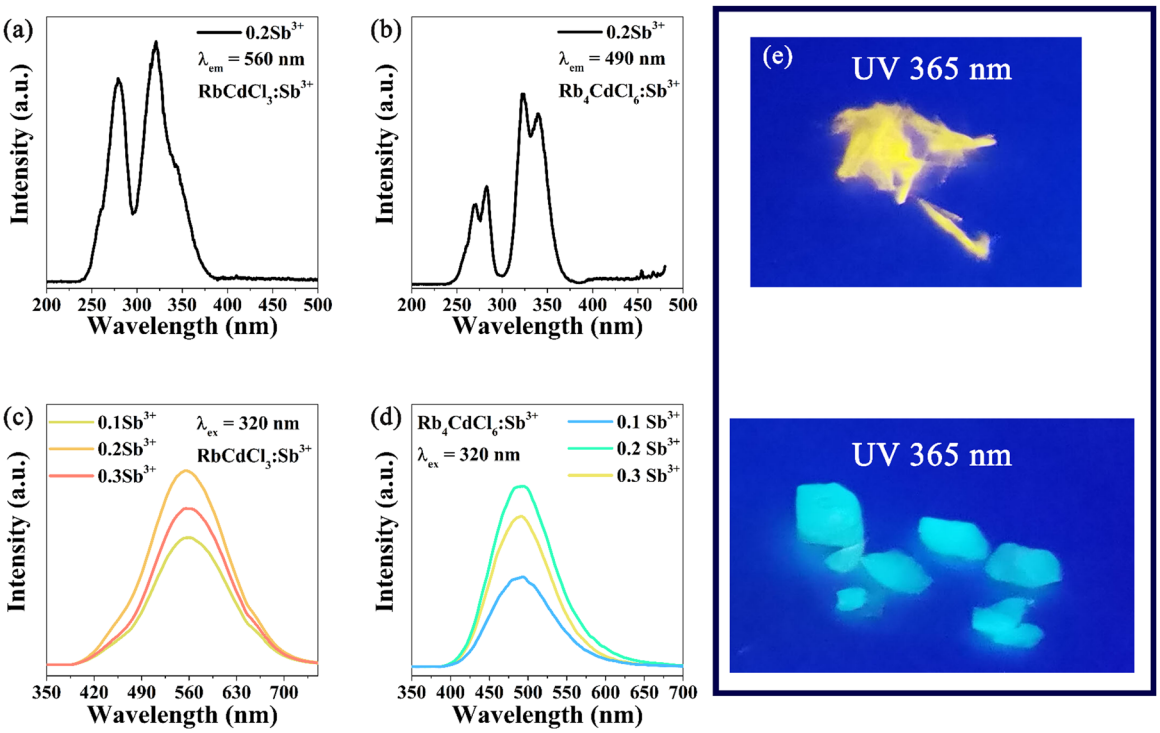

Fig. 4 (a) and (b) PLE of the $RbCdCl_3:Sb^{3+}$ and $Rb_4CdCl_6:Sb^{3+}$ crystals, respectively. (c) and (d) PL of the $RbCdCl_3:Sb^{3+}$ and $Rb_4CdCl_6:Sb^{3+}$ crystals, respectively. (e) Luminescence photos of $RbCdCl_3:Sb^{3+}$ and $Rb_4CdCl_6:Sb^{3+}$ crystals under ultraviolet light irradiation at 365 nm.

excitation band at 320 nm. $Rb_4CdCl_6:Sb^{3+}$ has cyan emission (490 nm) under 320 nm excitation (Fig. 4d). However, $RbCdCl_3:Sb^{3+}$ has broadband yellow emission (560 nm) under 320 nm excitation (Fig. 4c). It was most likely dopant-induced STEs in the $[SbCl_6]^{3-}$ polyhedrons that were responsible for the related broad emissions in the 400–700 nm region under 320 nm excitation. Photographs of the luminescence of the $RbCdCl_3:Sb^{3+}$ and $Rb_4CdCl_6:Sb^{3+}$ materials under 365 nm excitation are shown in Fig. 4e.

The dynamic process of electronic changes was then investigated. When the $RbCdCl_3:Sb^{3+}$ crystals were excited at 320 nm, their broad emission showed a gradual decline with a long lifetime of 7.9 μs, which is compatible with the STE emission (Fig. 5a). The STE emission of the $Rb_4CdCl_6:Sb^{3+}$ crystals had a lifetime of 4.2 μs, which was a little bit shorter than that of $RbCdCl_3:Sb^{3+}$(Fig. 5b). This energy transfer from the host to Sb^{3+} could be accelerated by increasing the concentration of Sb^{3+} dopant.[9]

In addition, we used temperature-dependent PL spectra to investigate the thermal stability of $RbCdCl_3:Sb^{3+}$ and $Rb_4CdCl_6:Sb^{3+}$ crystals. Fig. 6a depicts the change in the PL spectra of $RbCdCl_3:Sb^{3+}$ with temperature in the −180 to 150 °C range. Interestingly, there was a double emission peak (460 and 560 nm) at low temperatures. The fact that isolated units exist

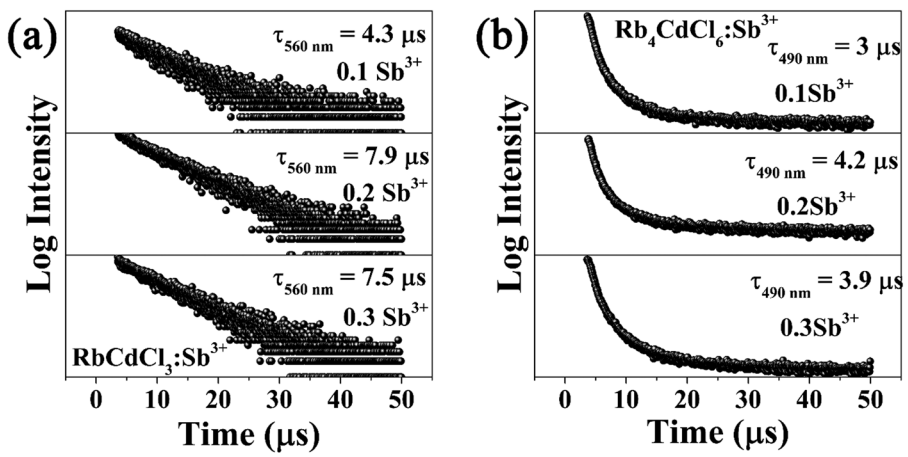

Fig. 5 (a) and (b) Decay curves of $RbCdCl_3:Sb^{3+}$ and $Rb_4CdCl_6:Sb^{3+}$ crystals, respectively.

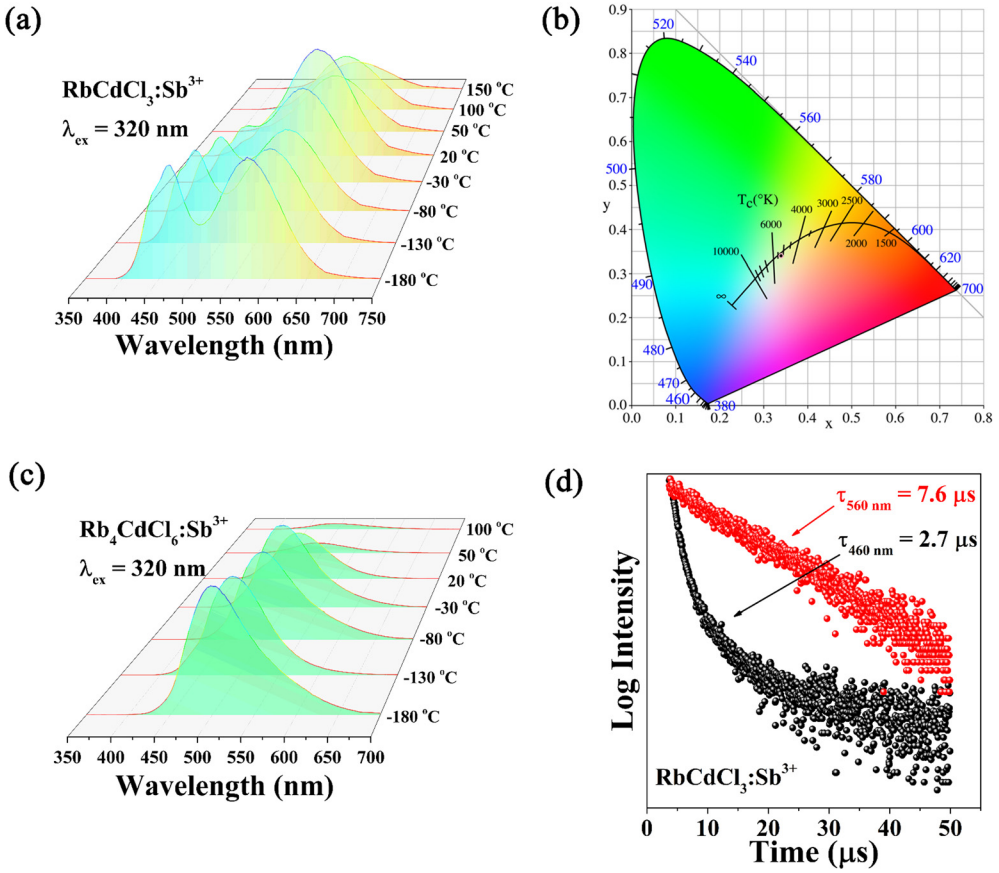

Fig. 6 (a) Temperature-dependent PL of $RbCdCl_3:Sb^{3+}$ crystals. (b) The corresponding CIE chromaticity coordinates of $RbCdCl_3:Sb^{3+}$ crystals at −180 °C. (c) Temperature-dependent PL of $Rb_4CdCl_6:Sb^{3+}$ crystals. (d) Decay curves of $RbCdCl_3:Sb^{3+}$ at −180 °C were monitored at 460 and 560 nm, respectively.

in the vacancy-ordered metal halides is largely responsible for this result, which shows that the emission processes of host STEs and dopant STEs are mutually independent. The $RbCdCl_3:Sb^{3+}$ crystals' double luminescence is also made possible by the little energy transfer from host to dopant STEs, which would otherwise extinguish the host emission. At this time, white light

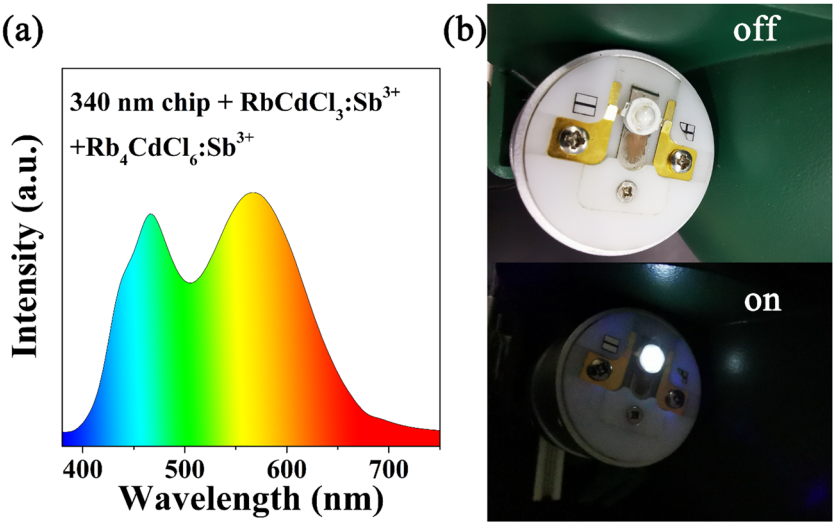

Fig. 7 (a) EL spectra with the composition 340 nm chip, yellow emission $RbCdCl_3:Sb^{3+}$, and cyan emission $Rb_4CdCl_6:Sb^{3+}$. (b) Photograph of the luminescence of the encapsulated LED device after applying current.

emission can be obtained by mixing blue light and yellow light (Fig. 6b). The intensity of the emission peak at 460 nm decreases rapidly with increasing temperature, however, the intensity of the emission peak at 560 nm decreases slowly and the intensity of the emission increases at a certain temperature (−30 to 20 °C). It is noteworthy that the intensity of the emission peaks of Sb^{3+} ions is well maintained relative to the charge transition band of the host. Fig. 6c demonstrates that the PL spectra of Rb_4CdCl_6:Sb^{3+} change as a function of temperature in the −180 to 100 °C range. The intensity of the emission peak at 490 nm decreases with increasing temperature and the peak position is blue-shifted. This phenomenon is common; as the temperature increases, the lattice of the Rb_4CdCl_6:Sb^{3+} material expands, resulting in a weakening of the crystal field strength, and the $^5S_2 \rightarrow {}^5S_1/{}^5P_1$ transition energy of Sb^{3+} increases as the crystal field strength decreases, resulting in a shift of the emission peaks towards higher energies.

Due to defects caused by the Sb^{3+} dopant, which disrupted the electron cloud and encouraged carrier entrapment in the nearby $[CdCl_6]^{4-}$ octahedra, as previously reported,[24] the charge transition band recombination was slowed down.[9] The $RbCdCl_3$:Sb^{3+} crystals displayed a double-exponential decay with a short component of 2.7 μs and a long component of 7.6 μs (Fig. 6d), which corresponded to the two emission components (460 and 560 nm). It is important to note that the Sb^{3+} dopant in metal halide structures was responsible for the lifetimes of the dopant STEs being essentially constant when the temperature varied. Finally, the light-emitting diode (LED) device is obtained by using both fabricated $RbCdCl_3$:Sb^{3+} (560 nm) and Rb_4CdCl_6:Sb^{3+} (490 nm) materials. LED device results show that a good color rendering index (91) and correlated color temperature (4303 K) can be obtained using synthetic $RbCdCl_3$:Sb^{3+} and Rb_4CdCl_6:Sb^{3+} materials (Fig. 7a and b).

4. Conclusions

In summary, the same reactor produces two distinct crystal types with various crystal phases and shapes. This process of simultaneous synthesis of materials is also distinctive. $RbCdCl_3$:Sb^{3+} needle-shaped crystals with yellow emission (560 nm) and Rb_4CdCl_6:Sb^{3+} bulk-shaped crystals with blue emission (460 nm) are synthesized. A new multi-resonance luminescence is found in Sb^{3+} doped $RbCdCl_3$ crystals at low temperatures. The bimodal emission of the $RbCdCl_3$:Sb^{3+} crystals is attributed to the host and dopant STEs, respectively. The crystal structure of the $RbCdCl_3$:Sb^{3+} metal halide is vacancy-ordered, which is principally responsible for the isolation of the host and dopant STEs. The temperature-dependent spectra demonstrate that energy transfers from the host to Sb^{3+} as temperature rises. White light emission is obtained at −180 °C, slowly changing to yellow light emission as the temperature increases. The simultaneous acquisition of $RbCdCl_3$:Sb^{3+} and Rb_4CdCl_6:Sb^{3+} crystals largely simplifies the synthesis process and adds members to the luminescent material family.

Conflicts of interest

There are no conflicts to declare.

Acknowledgements

This work is financially supported by the National Key Research and Development Program of China (2022YFB3503800), the National Natural Science Foundation of China (NSFC no. 51932009, 51902226, 52172166, U2005212), the Natural Science Fund of Heilongjiang Province (LH2019F013), the 111 Project (B13015) of Ministry Education of China to Harbin Engineering University, and the Project of High-level Scientific Research Guidance of Harbin Engineering University (no. 3072022TS2508).

Notes and references

1 K. Han, J. Jin, B. Su and Z. Xia, *Trends Chem.*, 2022, **4**, 1034–1044.
2 K. Han, J. Qiao, S. Zhang, B. Su, B. Lou, C. G. Ma and Z. Xia, *Laser Photonics Rev.*, 2023, **17**, 2200458.
3 L.-y Huang and W. R. Lambrecht, *Phys. Rev. B: Condens. Matter Mater. Phys.*, 2013, **88**, 165203.
4 J. Mao, H. Lin, F. Ye, M. Qin, J. M. Burkhartsmeyer, H. Zhang, X. Lu, K. S. Wong and W. C. Choy, *ACS Nano*, 2018, **12**, 10486–10492.
5 S. Pimputkar, J. S. Speck, S. P. DenBaars and S. Nakamura, *Nat. Photonics*, 2009, **3**, 180–182.
6 C. Bi, Z. Yao, J. Hu, X. Wang, M. Zhang, S. Tian, A. Liu, Y. Lu, N. H. de Leeuw, M. Sui and J. Tian, *ACS Energy Lett.*, 2023, **8**, 731–739.
7 B. Wang, Y. H. Zhou, S. Yuan, Y. H. Lou, K. L. Wang, Y. Xia, C. H. Chen, J. Chen, Y. R. Shi, Z. K. Wang and L. S. Liao, *Angew. Chem.*, 2023, e202219255.
8 G. Zhou, B. Su, J. Huang, Q. Zhang and Z. Xia, *Mater. Sci. Eng., R*, 2020, **141**, 100548.
9 B. Chen, Y. Guo, Y. Wang, Z. Liu, Q. Wei, S. Wang, A. L. Rogach, G. Xing, P. Shi and F. Wang, *J. Am. Chem. Soc.*, 2021, **143**, 17599–17606.
10 Z. Tan, J. Li, C. Zhang, Z. Li, Q. Hu, Z. Xiao, T. Kamiya, H. Hosono, G. Niu, E. Lifshitz, Y. Cheng and J. Tang, *Adv. Funct. Mater.*, 2018, **28**, 1801131.
11 D. Huang, Q. Ouyang, Y. Kong, B. Wang, Z. Cheng, A. A. Al Kheraif, H. Lian and J. Lin, *Dalton Trans.*, 2023, **52**, 5715–5723.
12 G. Zhang, P. Dang, H. Xiao, H. Lian, S. Liang, L. Yang, Z. Cheng, G. Li and J. Lin, *Adv. Opt. Mater.*, 2021, **9**, 2101637.
13 J. Jin, Y. Peng, Y. Xu, K. Han, A. Zhang, X.-B. Yang and Z. Xia, *Chem. Mater.*, 2022, **34**, 5717–5725.
14 Y. Jing, Y. Liu, X. Jiang, M. S. Molokeev, Z. Lin and Z. Xia, *Chem. Mater.*, 2020, **32**, 5327–5334.
15 Y. Jing, Y. Liu, M. Li and Z. Xia, *Adv. Opt. Mater.*, 2021, **9**, 2002213.

16 Y. Jing, Y. Liu, J. Zhao and Z. Xia, *J. Phys. Chem. Lett.*, 2019, **10**, 7439–7444.
17 B. Su, M. Li, E. Song and Z. Xia, *Adv. Funct. Mater.*, 2021, **31**, 2105316.
18 Q. Wei, T. Chang, R. Zeng, S. Cao, J. Zhao, X. Han, L. Wang and B. Zou, *J. Phys. Chem. Lett.*, 2021, **12**, 7091–7099.
19 J.-B. Luo, J.-H. Wei, Z.-Z. Zhang and D.-B. Kuang, *Inorg. Chem.*, 2022, **61**, 338–345.
20 J. Nie, B. Zhou, S. Fang, H. Zhong, H. Li and Y. Shi, *Chem. Mater.*, 2022, **34**, 6288–6295.
21 D.-Y. Li, J.-H. Song, Y. Cheng, X.-M. Wu, Y.-Y. Wang, C.-J. Sun, C.-Y. Yue and X.-W. Lei, *Angew. Chem., Int. Ed.*, 2022, **134**, e202206437.
22 A. Zhang, J. Jin and Z. Xia, *Adv. Opt. Mater.*, 2022, **10**, 2200720.
23 D.-Y. Li, J.-H. Song, Z.-Y. Xu, Y.-J. Gao, X. Yin, Y.-H. Hou, L.-J. Feng, C.-Y. Yue, H. Fei and X.-W. Lei, *Chem. Mater.*, 2022, **34**, 6985–6995.
24 Q.-L. Wei, X.-F. Meng, W.-C. Lin, S.-G. Ge, X.-X. Han, L. Chen, R.-S. Zeng and B. S. Zou, *J. Phys. Chem. Mater.*, 2022, **13**, 8436–8446.